On-Chip Generation and Manipulation of Entangled Photons Based on Reconfigurable Lithium-Niobate Waveguide Circuits

H. Jin,[1] F. M. Liu,[2] P. Xu,[1,*] J. L. Xia,[2] M. L. Zhong,[1] Y. Yuan,[1] J. W. Zhou,[2] Y. X. Gong,[3] W. Wang,[2] and S. N. Zhu[1]

[1]*National Laboratory of Solid State Microstructures and College of Physics, Collaborative Innovation Center of Advanced Microstructures, Nanjing University, Nanjing 210093, China*
[2]*Beijing Institute of Aerospace Control Devices, Beijing 100094, China*
[3]*Department of Physics, Southeast University, Nanjing 211189, China*

A consequent tendency toward high-performance quantum information processing is to develop the fully integrated photonic chip. Here, we report the on-chip generation and manipulation of entangled photons based on reconfigurable lithium-niobate waveguide circuits. By introducing a periodically poled structure into the waveguide circuits, two individual photon-pair sources with a controllable electro-optic phase shift are produced within a Hong-Ou-Mandel interferometer, resulting in a deterministically separated identical photon pair. The state is characterized by $92.9 \pm 0.9\%$ visibility Hong-Ou-Mandel interference. The photon flux reaches $\sim 1.4 \times 10^7$ pairs $nm^{-1}\,mW^{-1}$. The whole chip is designed to contain nine similar units to produce identical photon pairs spanning the telecom C and L band by the flexible engineering of nonlinearity. Our work presents a scenario for on-chip engineering of different photon sources and paves the way to fully integrated quantum technologies.

Tremendous progress has been achieved in integrated photonic circuits [1–10], providing a solid strategy for high-performance quantum information processing. To increase the integration complexity, further integration of photon sources together with the photonic circuits are of essential importance [11–13]. For practical applications, strategic effort should be devoted to developing the photonic chip's characteristics of low energy cost, high-efficiency internal photon sources, and fast and convenient phase modulation for enabling multiple high-fidelity quantum operations on a single chip. Therefore, integrated optical materials capable of producing and manipulating entangled photons are highly desired, and these will become pivotal ingredients for fully integrated quantum technologies.

The lithium-niobate (LN) crystal, also called the "silicon of photonics" [14,15], belongs to one of the valuable materials for integrated quantum optics, owing to strong $\chi^{(2)}$ nonlinearity, large piezoelectric, acousto-optic and electro-optic coefficient features, as well as the well-developed waveguide fabrication technique using either the proton-exchange or the titanium-indiffusion method. In telecommunications applications, the LN modulators based on electro-optic effect have reached 40 GHz (100 GHz in the laboratory [16]) and have recently been demonstrated for fast path and polarization control of single photons [17]. More specifically, a domain-engineering technique [18,19] can be introduced to LN, leading to the desirable quasi-phase-matching (QPM) spontaneous parametric down-conversion (SPDC) process for efficient generation of entangled photons. When complex designs of the poling structure are considered, multiple operations on entangled

sources can be achieved on a single bulk crystal platform [20,21]. When the bulk LN is further fabricated into the waveguide structure, the photon flux will be greatly enhanced, as was first demonstrated from a single periodically poled LN (PPLN) waveguide [22,23]. Considering the recently developed quantum memory [24] in a LN waveguide, the LN is promising for photonic chips with a complete family of robust, integrated quantum devices.

All the aforementioned features allow complex waveguide circuits embedded with high-flux photon sources and fast phase shifters on a single LN chip, which makes LN qualified for more complex quantum tasks. Here, based on a single LN photonic chip we demonstrate the generation and deterministic separation of an identical photon pair at telecom wavelengths. The deterministically separated identical photon pair is characterized by $92.9 \pm 0.9\%$ visibility Hong-Ou-Mandel (HOM) interference. The photon flux reaches $\sim 1.4 \times 10^7$ pairs $nm^{-1}\,mW^{-1}$. Continuous morphing from a two-photon separated state to a bunched state is further demonstrated by on-chip fast control of electro-optic phase shift (EOPS). The whole chip is designed to contain nine similar units to produce identical photon pairs spanning the telecom C and L band by the flexible engineering of nonlinearity. These results denote that the LN photonic chip is competent for practical applications of fully integrated quantum technologies with low energy cost, high-efficiency and flexible internal photon sources, fast and convenient phase modulators, and reconfigurable waveguide circuits.

Figure [1(a)] shows the main structure of this chip. Basically, it is composed of annealed proton exchanged channel waveguides integrated on a Z-cut PPLN crystal.
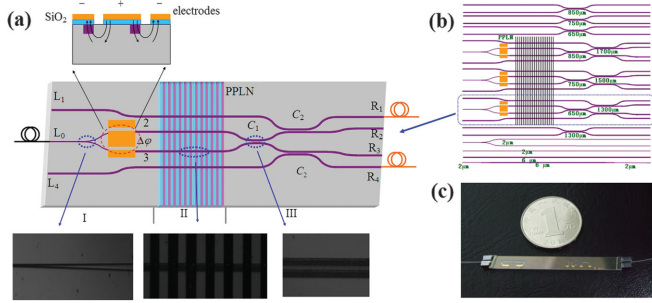
FIG. 1 (color). (a) The photonic chip with dimensions of 50 mm × 5 mm × 0.5 mm. The widths of single mode waveguides are 2 μm for the pump and 6 μm for entangled photons. The periodically poled section is 10 mm long with a period of 15.32 μm. The interaction length of C_1/C_2 is 650 μm/1300 μm at a gap of 4 μm. The upper inset is the structure of the electro-optic modulator. The electrode pairs are 8.35 mm long with a separation of 6 μm. The buffer layer (SiO_2) is etched along the gap between the electrodes to suppress dc drift. The lower three insets are the micrographs of the Y branch, the PPLN waveguide, and the directional coupler, respectively. (b) The whole structure of the chip. (c) Photograph of the chip with fixed fiber pigtails.

This design enables the generation, interference, and filtering of entangled photons from separate regions of PPLN waveguides, leading to reconfigurable on-chip quantum light sources. The chip can be characterized by three sections. Section I is designed to deal with the classical pump light. A 780 nm pump is coupled into waveguide L_0 and equally distributed by a Y-branch single mode beam splitter at the wavelength of 780 nm. After the Y branch, the electro-optic effect is considered to control the phase shift between two paths. Electrodes are fabricated above two pump waveguides for applying a voltage. Transition tapers then follow to connect the 780 nm Y branch with the 1560 nm single mode waveguides. Section II is the PPLN region, in which degenerate photon pairs at 1560 nm are generated indistinguishably from either one of the two PPLN waveguides, yielding a path-entangled state $(|2, 0\rangle + e^{i\Delta\varphi}|0, 2\rangle)/\sqrt{2}$. The relative phase $\Delta\varphi$ is transferred from the phase difference of pump modes. In section III, quantum interference is realized by a 2 × 2 directional coupler (C_1). The on-chip phase is adjusted by changing the voltage applied in section I. The entangled photons are separated from the pump by on-chip wavelength filters (C_2). Entangled photons are transferred to the neighboring waveguides R_1 and R_4. The pump is left in R_2 and R_3. The input waveguide L_0 and output waveguides R_1 and R_4 are directly connected with optical fiber tips, which are fixed with the chip by using UV-curing adhesive after reaching a high coupling efficiency. This removes the need for optimizing the coupling during the observation of quantum interference.

When the phase shift $\Delta\varphi$ between pump modes in waveguide 2 and 3 is zero, the chip worked as a balanced

time-reversed Hong-Ou-Mandel (BRHOM) interferometer, realizing a deterministic separation (sep) of an identical 1560 nm photon pair,

$$\frac{1}{\sqrt{2}}(|2, 0\rangle + |0, 2\rangle) \overset{\text{BRHOM}}{\rightarrow} |1, 1\rangle. \qquad (1)$$

In this case, the photon pair always emits from different waveguides (one from R_1 and the other from R_4), marked as $|\Psi\rangle_{\text{sep}} = |1, 1\rangle$.

In a more general case, when the electro-optic phase shift $\Delta\phi$ is introduced, the state evolution in the chip can be written as

$$\frac{1}{\sqrt{2}}(|2, 0\rangle + e^{i\Delta\phi}|0, 2\rangle) \overset{\text{EOPS}}{\rightarrow} \frac{1}{\sqrt{2}}(|2, 0\rangle - |0, 2\rangle) \sin(\Delta\phi/2)$$
$$+ |1, 1\rangle \cos(\Delta\phi/2). \qquad (2)$$

The output state is a superposition of the two-photon separated state $|\Psi\rangle_{\text{sep}} = |1, 1\rangle$ ($\Delta\phi = 0$) and the bunched state $|\Psi\rangle_{\text{bunch}} = 1/\sqrt{2}(|2, 0\rangle - |0, 2\rangle)$ ($\Delta\varphi = \pi$, the photon pair always emits together from either R_1 or R_4). By varying the bias voltage U, and thus the phase difference, we will observe a continuous evolution from the two-photon separated state to the bunched state. Specifically, the photon-pair rate from R_1 and R_4 follows

$$P_{\text{sep}} \propto \cos^2(\Delta\phi/2) = \cos^2(\pi U/2V_\pi), \qquad (3)$$

while the photon-pair rate from R_1 or R_4 gives

$$P_{\text{bunch}} \propto \sin^2(\Delta\phi/2) = \sin^2(\pi U/2V_\pi). \qquad (4)$$

$V_\pi = \lambda_p d/2\Gamma\gamma_{33}n_p^3 L$ is a half-wave voltage, in which Γ is a fill factor reflecting the overlap between the electric field and the optical mode field [25], γ_{33} is the electro-optic coefficient, n_p and λ_p are the refractive index and wavelength of the pump, and L and d are the length and separation of electrode pairs. Here we design the electrodes as the push-pull configuration; i.e., two waveguides both experience the electric field but with different sign, so the effective electrode length should be $2L$.

Actually, as shown in Fig. 1(b), the LN chip contains three main photonic circuits, and each one has a structure similar to Fig. 1(a). The difference lying among three main circuits is the interaction lengths of C_1 and C_2. Different interaction lengths, including 650 and 1300 μm, 750 and 1500 μm, and 850 and 1700 μm, are designed to ensure a good splitting ratio for photon pairs. The dashed rectangle region indicates the one we use in this experiment, with the interaction lengths of 650 μm for C_1 and 1300 μm for C_2. Additionally, we also design the involved waveguide elements like single mode waveguides for 780 and 1560 nm, directional couplers, etc. around the three main photonic circuits for testing and optimizing the waveguide

fabrication technology. Figure 1(c) shows a photograph of the chip with fixed fiber pigtails.

Experimentally, the transformation from a two-photon bunched state to a separated one is observed by making coincidence counting measurements on R_1 and R_4 under different bias voltage. The experimental setup is sketched in Fig. 2(a). The photonic chip is temperature controlled at 25.5 °C. The 780 nm pump is a continuous-wave fiber laser that is polarization controlled and connected with input fiber L_0. We make coincidence counting measurement between R_1 and R_4, R_1 and R_1, and R_4 and R_4. The measured pump suppression is 29.2 dB for R_1 and 31.4 dB for R_4, which mainly arises from the integrated filters and the propagation losses in the waveguide. The pump is further suppressed by interference filters centered at 1560 nm which are inserted into the fiber delay lines [as shown in Fig. 2(a)]. The coincidence counts are recorded in Figs. 2(b)–2(d), respectively, exhibiting interference fringes with the visibilities of $98.9 \pm 0.3\%$, $97.5 \pm 0.9\%$, and $88.4 \pm 2.1\%$, respectively. The visibility is calculated by $V = (R_{\max} - R_{\min})/(R_{\max} + R_{\min})$, in which $R_{\max}$ and $R_{\min}$ are the maximum and minimum values of fitting. The accidental coincidence counts have been excluded. The period of these fringes is 7.1 V, giving the half-wave voltage $V_\pi = 3.55$ V. These fringes agree with Eq. (2) except that it is not a clean separated state $|\Psi\rangle_{\mathrm{sep}} = |1, 1\rangle$ when $U = 0$. From Fig. 2(b), the $|1, 1\rangle$ state is obtained when $U_{\mathrm{offset}} = 2.3$ V, namely, the offset bias voltage. This results from certain optical path difference between two PPLN waveguides. Here the difference between the visibilities of R_1 and R_1 and R_4 and R_4 is mainly caused by the imperfect coupling efficiency of $C_1(T \sim 54\%)$ and different losses in waveguides 2 and 3. The different losses make the two-photon state $(|2, 0\rangle + \alpha e^{i\Delta\phi}|0, 2\rangle)/\sqrt{2}$ before C_1, in which α stands for relative loss. When the photons interfere on C_1, the visibilities for the separated and bunched states are $V_{\mathrm{sep}}^{(1,4)} = 2\alpha/(1 + \alpha^2)$, $V_{\mathrm{bunch}}^{(1)} = 2\alpha T(1 - T)/[T^2 + \alpha^2(1 - T)^2]$, $V_{\mathrm{bunch}}^{(4)} = 2\alpha T(1 - T)/[\alpha^2 T^2 + (1 - T)^2]$. This imperfect coupling efficiency can be further optimized when applying a voltage to C_1. The small deviation between the positions of peaks in Fig. 2(b) and the dips in Figs. 2(c) and 2(d) is attributed to dc drift associated with the buffer layer (SiO$_2$) [26,27]. Here the dc drift has been depressed a lot by etching a groove on the SiO$_2$ buffer layer as shown in the inset of Fig. 1(a). The dc drift can be further minimized by replacing SiO$_2$ with a transparent conductive buffer layer such as indium tin oxide [27].

According to the above measurement, we configured the chip to emit a $|1, 1\rangle$ state by controlling the voltage at 2.3 V. To evaluate the quality of such a state, we performed a HOM interference experiment by an external fiber beam splitter. The experimental setup is sketched in Fig. 3(a). Photons from R_1 and R_4 are sent into two fibers, one with a variable
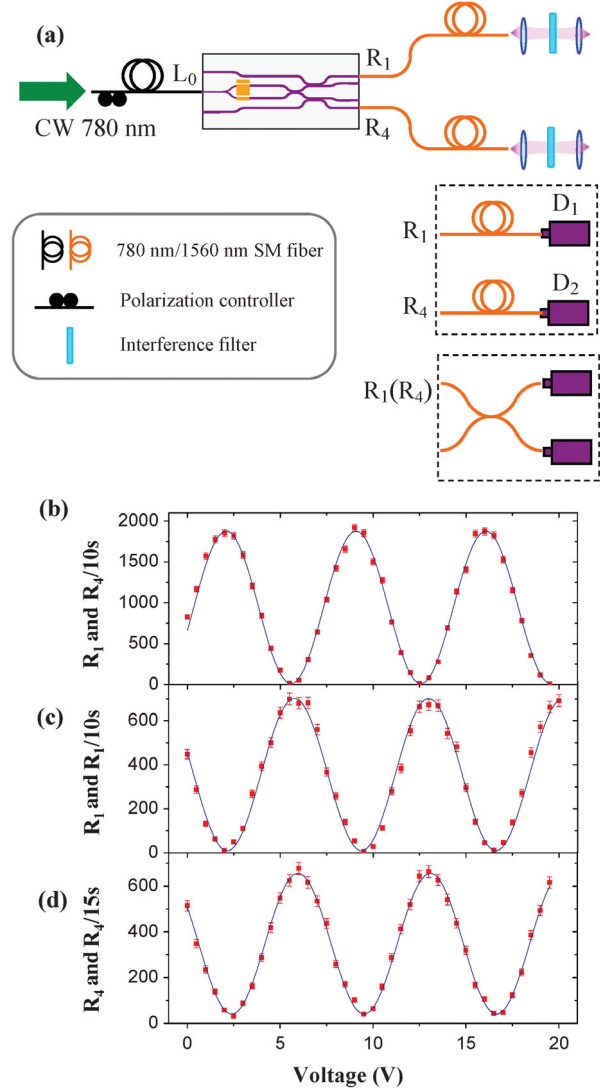

FIG. 2 (color). (a) Experimental setup of on-chip two-photon interference. The fiber laser is polarization controlled and connected with the input fiber L_0. Before single-photon detectors, 14 nm bandwidth interference filters centered at 1560 nm are used to further eliminate the pump. The coincidence counting measurements are made between R_1 and R_4, R_1 and R_1, and R_4 and R_4, respectively. The results are recorded in (b)–(d). The solid lines are sinusoidal fitting, and error bars show $\pm\sqrt{\text{counts}}$.

delay line in free space and the other with a polarization controller. Therefore, the indistinguishability of two photons in the arrival time and polarization can be ensured when they interfere on the fiber beam splitter. Figure 3(b) shows the coincidence counts that we recorded while varying the displacement of the free-space delay line. We observed a HOM dip with a visibility of $92.9 \pm 0.9\%$ after excluding the accidental coincidence counts. The nonideal visibility indicates that $|\Psi\rangle_{\mathrm{sep}}$ is not absolutely clean, containing some bunched portion [as shown in Fig. 2(d)] as well as some polarization rotations in the external single mode fibers which are not compensated perfectly.
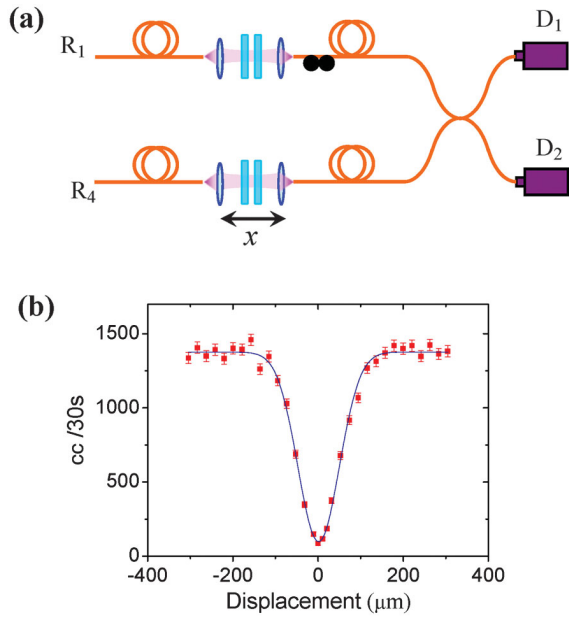
(a)

(b)

FIG. 3 (color). (a) Experimental setup of HOM interference. The photonic chip is controlled to emit separated photon pairs. In each arm there are two interference filters of 14 nm bandwidth. (b) Coincidence counts (cc) versus the displacement of the free-space delay line. Error bars show $\pm\sqrt{\text{counts}}$.

To evaluate the conversion efficiency of our device, we configure the chip to emit a separated state and measure the photon pairs picked out by an interference filter with 14 nm bandwidth. Two single counting rates were $R_1 = 40\,000$ Hz and $R_4 = 29\,000$ Hz, and the coincidence counting rate was $R_{cc} = 186$ Hz when the pump power coupled into the waveguide L_0 is 31 μW. The production rate of photon pairs in the PPLN waveguides reached $\sim 6.2 \times 10^6$ Hz (calculated by $N = R_1 R_4 / R_{cc}$). The production rate of photon pairs per units bandwidth and pump power was $\sim 1.4 \times 10^7$ Hz nm^{-1} mW^{-1} for the PPLN waveguide source of 10 mm length. The conversion efficiency reaches $N/N_{\text{pump}} = 5 \times 10^{-8}$. The total loss experienced by a photon exiting from R_1 or R_4 is 21.9 and 23.3 dB [calculated by $-10\log(R_{cc}/R_{1(4)})$], respectively, including the propagation loss in waveguides, the coupling efficiency from the chip to fiber, the filtering efficiencies, and the detector efficiencies. The coupling efficiency from the chip to the fiber is 1 dB. The total transmission efficiency of the fiber-free space-fiber filtering system (as shown in Fig. 2) is 30% (5.2 dB loss) including the 60% collection efficiency and 50% transmission efficiency of the 1560 nm interference filter. The detectors are set to give 9.2 and 8.5 dB loss, respectively. Thus, we can calculate the propagation loss of entangled photons in waveguides to be 6.5 dB for R_1 and 8.6 dB for R_4. The low propagation efficiency (compared with Refs. [28,29]) may result from the random scratches or other defects during the sample fabrication. However, the

propagation efficiency as well as the efficiencies of detectors and filtering systems can be further optimized.

The PPLN is the key section of this photonic chip, providing a flexible and feasible on-chip photon source. Here, by varying the poling period Λ, we actually design nine units on a 3-in. LN wafer as shown in Fig. 4(a), intending to generate identical photon pairs whose wavelengths cover the C band (1530–1565 nm) and L band (1565–1625 nm) in fiber communication. Each channel contains the same waveguide circuits as shown in Fig. 1(b) but different poling period, ranging from 14.36 μm to 16.28 μm in a step of 0.24 μm (the corresponding SPDC process at room temperature will produce identical photon pairs around 1560 nm by $\sim$12 nm separation). In this measurement, we verify the poling period and corresponding photon-pair wavelength by second harmonic generation (SHG), the inversed one of spontaneous parametric down-conversion in the assistant waveguide (L_1 or L_4). Figure 4(b) shows the wavelengths for efficient SHG in different channels at room temperature (25.5 °C). In this work we choose the fifth unit with the poling period of 15.32 μm. From this chip, the two-color photon pair is also accessible by increasing the working temperature due to the QPM condition of PPLN.

Recently, a related work was published [11]. It makes a great step toward fully integrated quantum optics by integrating entangled photons by four-wave mixing processes together with waveguide circuits on a silicon-on-insulator photonic chip. Silicon materials are considered to be competitive for quantum photonic devices for the mature fabrication technologies and accessible four-wave mixing photon sources [30–35]. But at the present stage, the nonlinearity and phase modulator still need to be improved. In contrast, although the LN circuits contain larger footprints and the fabrication technology is not compatible with CMOS electronics, it contains efficient PPLN waveguide photon sources and fast electro-optic modulators, which makes it quite competent for on-chip engineering of quantum light sources. By a careful design of QPM sections, the polarization, frequency, spatial mode, and path degrees of freedom can be engineered during the SPDC processes. The efficient identical photon pair demonstrated here will stimulate the heralded generation of single photon sources [36] as well as the extension to the multiphoton fashion. When associated with phase-controlled circuits, more types of quantum light sources can be exploited in addition to the on-chip quantum information processing. This will pave a new way for the fully integrated quantum optics. Additionally, the LN photonic chip can act as an alternative platform for quantum walk, especially when the nonlinear PPLN section is embedded [37,38], which may bring new characteristics to quantum walk and stimulate further applications in quantum computing.
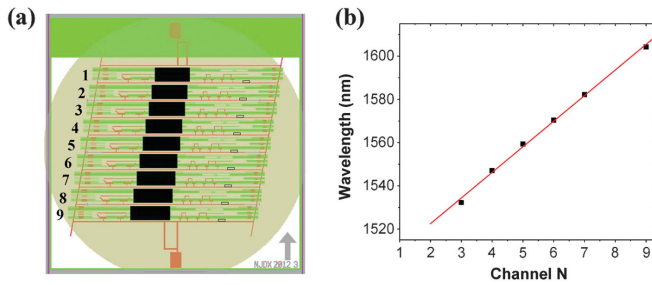
FIG. 4 (color).   (a) The layout of nine channels with the same waveguide circuits but different poling periods on a LN wafer. (b) Efficient SHG wavelengths in different channels at 25.5 °C. The red line is a linear fitting.

*Corresponding author.
pingxu520@nju.edu.cn

[1] A. Politi, M. J. Cryan, J. G. Rarity, S. Yu, and J. L. O'Brien, Science **320**, 646 (2008).
[2] J. L. O'Brien, A. Furusawa, and J. Vuckovic, Nat. Photonics **3**, 687 (2009).
[3] J. C. F. Matthews, A. Politi, A. Stefanov, and J. L. O'Brien, Nat. Photonics **3**, 346 (2009).
[4] A. Politi, J. C. F. Matthews, and J. L. O'Brien, Science **325**, 1221 (2009).
[5] B. J. Smith, D. Kundys, N. Thomas-Peter, P. G. R. Smith, and I. A. Walmsley, Opt. Express **17**, 13516 (2009).
[6] S. Tanzilli, A. Martin, F. Kaiser, M. P. De Micheli, O. Alibart, and D. B. Ostrowsky, Laser Photonics Rev. **6**, 115 (2012).
[7] P. J. Shadbolt, M. R. Verde, A. Peruzzo, A. Politi, A. Laing, M. Lobino, J. C. F. Matthews, M. G. Thompson, and J. L. O'Brien, Nat. Photonics **6**, 45 (2011).
[8] B. J. Metcalf et al., Nat. Commun. **4**, 1356 (2013).
[9] M. Tillmann, B. Dakić, R. Heilmann, S. Nolte, A. Szameit, and P. Walther, Nat. Photonics **7**, 540 (2013).
[10] A. Crespi, R. Osellame, R. Ramponi, D. J. Brod, E. F. Galvão, N. Spagnolo, C. Vitelli, E. Maiorino, P. Mataloni, and F. Sciarrino, Nat. Photonics **7**, 545 (2013).
[11] J. W. Silverstone et al., Nat. Photonics **8**, 104 (2014).
[12] A. Martin, O. Alibart, M. P. De Micheli, D. B. Ostrowsky, and S. Tanzilli, New J. Phys. **14**, 025002 (2012).
[13] N. Matsuda, H. L. Jeannic, H. Fukuda, T. Tsuchizawa, W. J. Munro, K. Shimizu, K. Yamada, Y. Tokura, and H. Takesue, Sci. Rep. **2**, 817 (2012).
[14] M. Kösters, B. Sturman, P. Werheit, D. Haertle, and K. Buse, Nat. Photonics **3**, 510 (2009).
[15] R. S. Weis and T. K. Gaylord, Appl. Phys. A **37**, 191 (1985).
[16] A. Kanno, T. Sakamoto, A. Chiba, T. Kawanishi, K. Higuma, M. Sudou, and J. Ichikawa, IEICE Electron. Express **7**, 817 (2010).
[17] D. Bonneau, M. Lobino, P. Jiang, C. M. Natarajan, M. G. Tanner, R. H. Hadfield, S. N. Dorenbos, V. Zwiller, M. G. Thompson, and J. L. O'Brien, Phys. Rev. Lett. **108**, 053601 (2012).
[18] J. A. Armstrong, N. Bloembergen, J. Ducuing, and P. S. Pershan, Phys. Rev. **127**, 1918 (1962).
[19] P. A. Franken and J. F. Ward, Rev. Mod. Phys. **35**, 23 (1963).
[20] H. Y. Leng, X. Q. Yu, Y. X. Gong, P. Xu, Z. D. Xie, H. Jin, C. Zhang, and S. N. Zhu, Nat. Commun. **2**, 429 (2011).
[21] H. Jin, P. Xu, X. W. Luo, H. Y. Leng, Y. X. Gong, W. J. Yu, M. L. Zhong, G. Zhao, and S. N. Zhu, Phys. Rev. Lett. **111**, 023603 (2013).
[22] S. Tanzilli, H. De Riedmatten, H. Tittel, H. Zbinden, P. Baldi, M. De Micheli, D. B. Ostrowsky, and N. Gisin, Electron. Lett. **37**, 26 (2001).
[23] K. Sanaka, K. Kawahara, and T. Kuga, Phys. Rev. Lett. **86**, 5620 (2001).
[24] E. Saglamyurek, N. Sinclair, J. Jin, J. A. Slater, D. Oblak, F. Bussières, M. George, R. Ricken, W. Sohler, and W. Tittel, Nature (London) **469**, 512 (2011).
[25] T. Fujiwara, A. Watanabe, and H. Mori, IEEE Photonics Technol. Lett. **2**, 260 (1990).
[26] S. Yamada and M. Minakata, Jpn. J. Appl. Phys. **20**, 733 (1981).
[27] C. M. Gee, G. D. Thurmond, H. Blauvelt, and H. W. Yen, Appl. Phys. Lett. **47**, 211 (1985).
[28] K. R. Parameswaran, M. Fujimura, M. H. Chou, and M. M. Fejer, IEEE Photonics Technol. Lett. **12**, 654 (2000).
[29] C. Langrock, S. Kumar, J. E. McGeehan, A. E. Willner, and M. M. Feijer, J. Lightwave Technol. **24**, 2579 (2006).
[30] J. E. Sharping, K. F. Lee, M. A. Foster, A. C. Turner, B. S. Schmidt, M. Lipson, A. L. Gaeta, and P. Kumar, Opt. Express **14**, 12388 (2006).
[31] S. Clemmen, K. Phan Huy, W. Bogaerts, R. G. Baets, Ph. Emplit, and S. Massar, Opt. Express **17**, 16558 (2009).
[32] H. Takesue, H. Fukuda, T. Tsuchizawa, T. Watanabe, K. Yamada, Y. Tokura, and S.-i. Itabashi, Opt. Express **16**, 5721 (2008).
[33] S. Azzini, D. Grassani, M. J. Strain, M. Sorel, L. G. Helt, J. E. Sipe, M. Liscidini, M. Galli, and D. Bajoni, Opt. Express **20**, 23100 (2012).
[34] C. Xiong et al., Opt. Lett. **36**, 3413 (2011).
[35] M. J. Collins et al., Nat. Commun. **4**, 2582 (2013).
[36] T. Meany, L. A. Ngah, M. J. Collins, A. S. Clark, R. J. Williams, B. J. Eggleton, M. J. Steel, M. J. Withford, O. Alibart, and S. Tanzilli, Laser Photonics Rev. **8**, L42 (2014).
[37] A. S. Solntsev, A. A. Sukhorukov, D. N. Neshev, and Y. S. Kivshar, Phys. Rev. Lett. **108**, 023601 (2012).
[38] M. Gräfe, A. S. Solntsev, R. Keil, A. A. Sukhorukov, M. Heinrich, A. Tünnermann, S. Nolte, A. Szameit, and Yu. S. Kivshar, Sci. Rep. **2**, 562 (2012).